Transportation Research Part C 124 (2021) 102918

Contents lists available at ScienceDirect

Transportation Research Part C

journal homepage: www.elsevier.com/locate/trc

A cooperative driving framework for urban arterials in mixed traffic conditions

Zhen Yang [a], Yiheng Feng [b,*], Henry X. Liu [a]

[a] Department of Civil and Environmental Engineering, University of Michigan, 2350 Hayward Street, Ann Arbor, MI 48109, United States
[b] Lyles School of Civil Engineering, Purdue University, 550 Stadium Mall Drive, West Lafayette, IN 47907, United States

ARTICLE INFO

Keywords:
Cooperative driving
Vehicle trajectory planning
Traffic signal optimization
Mixed traffic condition

ABSTRACT

Enabling technologies of connected and automated vehicles (CAVs) bring new opportunities to signalized intersection control. CAVs not only provide a new source of data for traffic management but also can be controlled as actuators to improve traffic flow. This study proposes a hierarchical and implementation-ready cooperative driving framework with a mixed traffic composition of CAVs, connected vehicles (CVs), and regular vehicles (RVs) for urban arterials. The proposed framework combines centralized and distributed control concepts, where the infrastructure generates optimal signal timing plans and provides high-level trajectory guidance to the CAVs while detailed trajectories are generated by each vehicle. The system consists of three levels of models. At the vehicle level, a state transition diagram is designed for different modes of operations of CAVs including eco-trajectory planning, cooperative adaptive cruise control (CACC) and collision avoidance. At the intersection level, a mixed-integer linear programming (MILP) problem is formulated to optimize the signal timing plan and arrival time of CAVs, with consideration of CACC platooning behaviors. At the corridor level, link performance functions are applied to calculate the total delay of the coordinated phases of each intersection, and a linear programming (LP) problem is formulated to optimize the offsets for every cycle, which are then passed to the intersection level. Simulation results from a calibrated real-world arterial corridor show that both mobility and fuel economy benefits from the cooperative driving framework. The total delay is reduced by 2.2%−33.0% and fuel consumption by 3.9%−7.4%, with different mixture of vehicle compositions and CAV penetration rates (e.g., 0%−100%). Sensitivity analysis on volume fluctuation is performed, which confirms the benefits of the dynamic offset optimization.

1. Introduction

Enabling technologies of connected and automated vehicles (CAVs) bring new opportunities to the urban transportation system, especially at signalized intersections, which are considered as the bottlenecks of the traffic network. CAVs not only provide a new source of data for traffic management but also can be controlled as actuators to improve traffic flow.

Leveraging proactively broadcast data (e.g., location and speed) from CAVs as a new data source, existing studies investigate how to improve the signal control system at different scales. Different methods are developed to adjust signal timing plans dynamically

* Corresponding author.
E-mail addresses: zhenyang@umich.edu (Z. Yang), feng333@purdue.edu (Y. Feng), henryliu@umich.edu (H.X. Liu).

https://doi.org/10.1016/j.trc.2020.102918
Received 9 May 2020; Received in revised form 27 September 2020; Accepted 1 December 2020
Available online 8 January 2021

based on traffic states measured from CAV data to optimize predefined performance measures (e.g., total delay, and throughput). For example, at the single intersection level, a two-level optimization problem is solved to minimize the total delay or queue length (Feng et al., 2015). At the corridor level, a simulation-based method is introduced to predict vehicle delay with trajectory data to optimize the signals, and results show the method outperforms coordinated actuated signal control (Goodall et al., 2013). At the network level, a distributed optimization approach is proposed to control traffic signals, assuming each intersection can receive CV data and exchange information with its neighboring intersections (Al Islam and Hajbabaie, 2017).

On the other hand, as actuators, CAVs can be controlled to form compact platoons such as cooperative adaptive cruise control (CACC) to improve mobility (Feng et al., 2019; Feng et al., 2019; Li et al., 2015). At signalized intersections, CAVs can plan vehicle trajectories in an energy-efficient way, with the traffic signal and traffic state information (i.e., eco-driving). In (He et al., 2015), to obtain the optimal vehicle trajectory, a multi-stage optimal control formulation is proposed with the consideration of vehicle queue and traffic signal status, for a single CAV. (Wang et al., 2017; Yang et al., 2016; Almannaa et al., 2019) focus on eco-CACC which optimizes the trajectories of CAV platoons. Not only is the trajectory of the platoon leading CAV optimized, the platoon splitting and merging behaviors are also considered. A field test is conducted in (Almannaa et al., 2019) that shows the benefits of eco-CACC.

In the past few years, researchers have proposed a new concept that integrates CAV-based signal optimization and CAV trajectory planning together, to further improve the intersection operation and reduce energy consumption. Li et al. are among the first to propose the idea of integrated optimization. In this work, CAVs follow the path optimized by signal controllers (Li et al., 2014). In (Xu et al., 2018), Xu et al. propose a two-level method, in which the upper level optimizes the signals and vehicle arrival time, and the lower level optimizes engine power and brake force. Yu et al. propose a comprehensive framework for the cooperative driving problem, which considers detailed signal parameters and vehicle trajectories with lane changing behavior at isolated intersections (Yu et al., 2018). In (Feng et al., 2018), a two-stage optimization problem is formulated, in which traffic signal is optimized with dynamic programming, and vehicle trajectory is controlled based on the optimal control theory. Yu et al. (Yu et al., 2019) extend the integrated control to a corridor level. A coordinated control mechanism of CAV trajectories is developed in a centralized formulation. A Mixed Integer Linear Programming (MILP) problem is formulated to plan the complete trajectory including both longitudinal and lateral behaviors of all the CAVs through the entire corridor given origins and destinations. However, all the above mentioned studies require a 100% CAV environment. Recently, integrated optimization in mixed traffic conditions is proposed by a few researchers. (Guo et al., 2019) considers the mixed traffic of CAVs and RVs and develop a two-step control framework, in which step one optimizes the signal timing plan with consideration of vehicle trajectories, and step two designs optimal trajectories with the optimal signal plan. The study from (Liu et al., 2019) prioritizes CACC platoons at intersections to improve the overall intersection performance. The objective of signal optimization is to maximize the throughput of the intersection. Information on RVs is estimated by the location and speed of CACC vehicles, which either cruise to pass the intersection or stop at the intersection with constant deceleration.

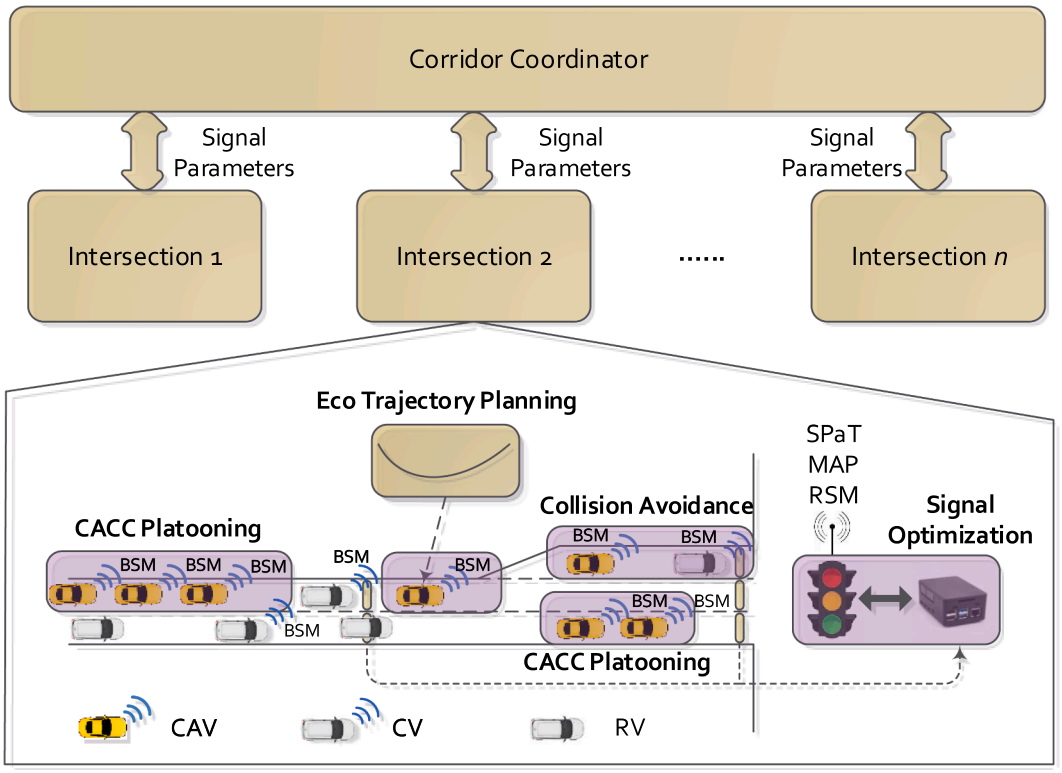

Fig. 1. Overview of Cooperative Driving Framework.

Although great achievements have been made in the area of CAV-based intersection management, existing studies suffer from three major limitations. The first limitation lies in the problem setup that in most of the studies, a 100% CAV environment is assumed (e.g., (Al Islam and Hajbabaie, 2017; He et al., 2015; Wang et al., 2017; Yang et al., 2016; Almannaa et al., 2019; Li et al., 2014; Xu et al., 2018; Yu et al., 2018; Feng et al., 2018; Yu et al., 2019), which requires all vehicles to be connected and highly automated (i.e., SAE Level 4 or higher). Second, usually a centralized problem is formulated (e.g., (Li et al., 2014; Yu et al., 2019; Guo et al., 2019). This requires heavily instrumented infrastructure with advanced sensors for infrastructure-based perception and high-performance computing (HPC) devices for real-time computation. Neither of these can be achieved shortly. A transition period from manually driven vehicles to CAVs will exist for a long time and current infrastructure with legacy sensors (e.g., loop-detectors) may even have longer lifecycles before being replaced. Finally, most of the studies are limited at isolated intersections or simply adding up single intersections without considering coordination (e.g., (Al Islam and Hajbabaie, 2017); (Liu et al., 2019)). However, an extensive literature has shown the importance of coordination at signalized corridors.

This study aims to address these limitations by proposing a hierarchical and implementation-ready cooperative driving framework with a mixed traffic composition of CAVs, connected vehicles (CVs), and regular vehicles (RVs). In our study, CAVs refer to vehicles that proactively broadcast information and can be controlled to generate specified trajectories. CVs and RVs are driven by human drivers, which are not controllable. However, CVs proactively broadcast information to other vehicles and the infrastructure, while RVs can only be observed by infrastructure detectors at fixed locations. A conceptual overview of the proposed cooperative driving framework is shown in Fig. 1. The infrastructure is responsible for collecting traffic information, estimating and predicting traffic states, controlling and coordinating traffic signals, and providing high-level trajectory guidance to CAVs, with the main objective of optimizing traffic flow and improving mobility. A bi-level structure is adopted in which a centralized Corridor Coordinator is combined with decentralized intersection level controllers. In the Corridor Coordinator, offsets of coordinated phases between consecutive intersections are optimized based on link performance functions to promote two-way coordination. At each intersection, CAV trajectory guidance in terms of the time of arrival and signal parameters (i.e., green split) are jointly optimized, given offset from the Corridor Coordinator and traffic states estimated from CAVs/CVs and/or loop detector data. Optimized signal timing plans and CAV time of arrival are broadcast in the form of signal phasing and timing (SPaT) messages and roadside safety messages (RSMs) respectively. On the vehicle level, each CAV is responsible for forming ad-hoc CACC platoons, generating detailed vehicle trajectories, and collision avoidance with CVs and RVs, with the main objective of ensuring safety and reducing fuel consumption and emissions. Meanwhile, both CAVs and CVs broadcast basic safety messages (BSMs).

The main features of the proposed framework include 1) It is designed for mixed traffic conditions, where CAVs, CVs, and RVs co-exist on the roadway. 2) It applies to the corridor level with multiple intersections. Coordination between intersections is explicitly modeled. 3) It is implementation-ready and does not require highly automated vehicles nor heavily instrumented infrastructure. Current commercial vehicles with advanced driving assistance systems (ADAS) such as GM Super Cruise and current infrastructure with loop detectors are sufficient to deploy the proposed cooperative driving functions. Other than that, only a wireless communication system (e.g., Dedicated Short Range Communication, cellular network, or hybrid) is required at both vehicle and infrastructure sides. The V2X communication network has been implemented and tested extensively in the past few years. 4) The proposed framework combines centralized and distributed control concepts, where the infrastructure provides high-level trajectory guidance to the CAVs while detailed trajectories are generated by each vehicle. This design can distribute the computational burden to achieve real-time performance, without expensive investments such as HPC. The major differences between the proposed framework and some existing studies are summarized in Table 1.

In the following, we will first introduce the overall system structure, and data flow of the proposed framework (Section 2), followed by detailed modeling approaches of the three levels: vehicle-level, intersection-level, and corridor-level (Sections 3 – 5). Then we will show simulation experiment results and comparison to the state-of-practice intersection management method to demonstrate the improvements and benefits (Section 6). Finally, Section 7 concludes the paper and lays out further research directions.

Table 1
Comparison between the proposed model and existing studies.

Literature	Traffic Signal Opt.	Vehicle Trajectory Opt.	CACC Platooning	Isolated Intersection	Corridor /Network Level	100% CAV PR	Mixed Traffic Condition
(Feng et al., 2015)	X			X			X
(Goodall et al., 2013)	X				X		X
(Al Islam and Hajbabaie, 2017)	X				X	X	
(He et al., 2015)		X		X		X	
(Wang et al., 2017; Yang et al., 2016; Almannaa et al., 2019)		X	X	X		X	
(Li et al., 2014; Xu et al., 2018; Yu et al., 2018; Feng et al., 2018)	X	X		X		X	
(Guo et al., 2019; Liang et al., 2020; Kamal et al., 2019)	X	X		X			X
(Yu et al., 2019)	X	X			X	X	
(Liu et al., 2019)	X	X	X	X			X
Our Study	X	X	X		X		X

2. Framework overview

In this section, the proposed system component diagram is described in detail. The system consists of three main components: roadway, intersection, and corridor as shown in Fig. 2, which correspond to the three conceptual levels in Fig. 1.

On the roadway, there are three types of vehicles: CAV, CV, and RV. All vehicles generate detector calls when they pass the loop-detectors, which are assumed to be installed at the entrance of each link. CAVs and CVs also broadcast BSMs to enable V2V and V2I communication. The longitudinal controls of the CAV are generated by the trajectory planning models, which include eco trajectory planning, CACC platooning behaviors, and adaptive cruise control (ACC). These models are introduced in Section 3. The trajectory planning models are not responsible for lateral maneuvers. If necessary lateral maneuvers are required (e.g., turning at intersections), the system would have to give vehicle control back to the driver.

At the intersection, after the RSU receives the data (i.e., BSM and detector data), the Vehicle Localization algorithm maps the BSM and detector data on the intersection map to identify lane, approach, and approaching signal phase (Feng, 2015). The Queuing Profile Prediction algorithm takes SPaT and approaching vehicle information from BSM and detectors to predict the queuing dynamics. The predicted queuing dynamics, SPAT data, and offset information from the corridor level are used to optimize the signal timing plan and the time of arrivals of CAVs, which are sent to the signal controllers to control the traffic signals and to CAVs to generate speed profiles, respectively. We consider that the RSU has computation capabilities to execute the optimization model. The details of the integrated optimization at the intersection level are introduced in section 4. The green splits of the coordinated phases of each intersection are sent to the corridor level for offset optimization, introduced in section 5. The offset optimization algorithm can either reside in one of the intersections (e.g., the master intersection) or at the traffic management center (TMC). The signal controllers at the intersection broadcast SPAT data and generate loop detector data.

3. Vehicle level models

In this section, vehicle level models are introduced. The vehicle level models are responsible for eco-trajectory planning, ad-hoc CACC platoon formation, and collision avoidance under uncertainties. Given the time of arrival from the infrastructure side (i.e., through V2I communication), each CAV plans its own trajectory. Ad-hoc CACC platoons can be formed, and split dynamically depending on the assigned time of arrival, vehicle position in the platoon, and behaviors of uncontrolled vehicles (i.e., CVs and RVs). For the leading vehicle in a CACC platoon, a trigonometric speed profile family is adopted and one of four eco scenarios (i.e., speed up, cruise, slow down, and stop) is chosen to generate an eco speed profile. To address the uncertainties in trajectory prediction, an adaptive cruise control (ACC) model is applied to each CAV as a safeguard to avoid collisions. To consolidate different behaviors of a CAV, a state transition diagram is designed to represent different operating modes and their transition relations. While notations are introduced in each section, a list of complete notations is provided in the Appendix for readers' convenience.

3.1. CAV states and transitions

Five states are defined for each CAV: free flow, intelligent follow, optimized control, stop, and launch. When a CAV platoon is approaching a signalized intersection, according to different traffic and signal conditions, it may experience different operating scenarios. A CAV platoon can be formed in two ways. First, when a group of CAVs enter the network in the same lane consecutively, a

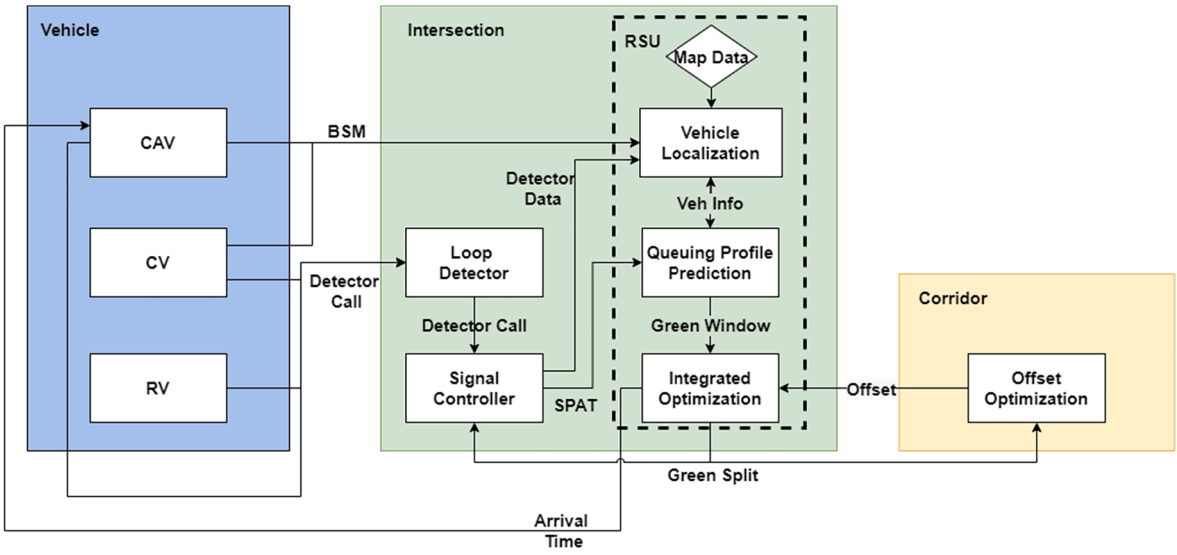

Fig. 2. System Component Diagram.

platoon will be naturally formed. Second, if the distance from a CAV to its leading CAV platoon becomes small, the CAV will merge into the leading platoon. This usually happens when the leading platoon slows down for the red light, or when an RV between the CAV and the platoon makes a lane change.

Different operating scenarios lead the CAVs to different states or transit from one state to another. The description of state transitions and corresponding triggers are shown in Fig. 3(a). The states are switched dynamically based on different criteria including vehicle speed, whether within communication range, car following distance, and traffic signal timing. To better illustrate the transitions, Fig. 3(b) shows a CAV platoon of three vehicles passing the intersection as an example, which describes the most common operating scenario. Before the CAVs enter the communication range, they are in the free-flow state. When the platoon enters the communication range, the leading vehicle (blue car) switches to the optimized control state, and the following vehicles (red cars) switch to the intelligent follow state. In the optimized control state, the leading CAV can choose one of four scenarios: accelerate (green dash line), cruise (cyan dash line), decelerate (orange dash line), and plan to stop (red line). In the figure, the platoon needs to stop after an RV (i.e., black car). When a CAV stops (e.g., $v < 5$ mph), it switches to the stop state. After the signal turns to green, the CAVs switch to the launch state and pass the intersection. Once the vehicle passes the intersection, it switches back to the free flow state. If a CAV doesn't need to stop, it switches directly from either optimized control or intelligent follow state to free-flow state after passing the intersection. In addition, in the intelligent follow state, if a CAV determines that its front vehicle can pass the intersection but it

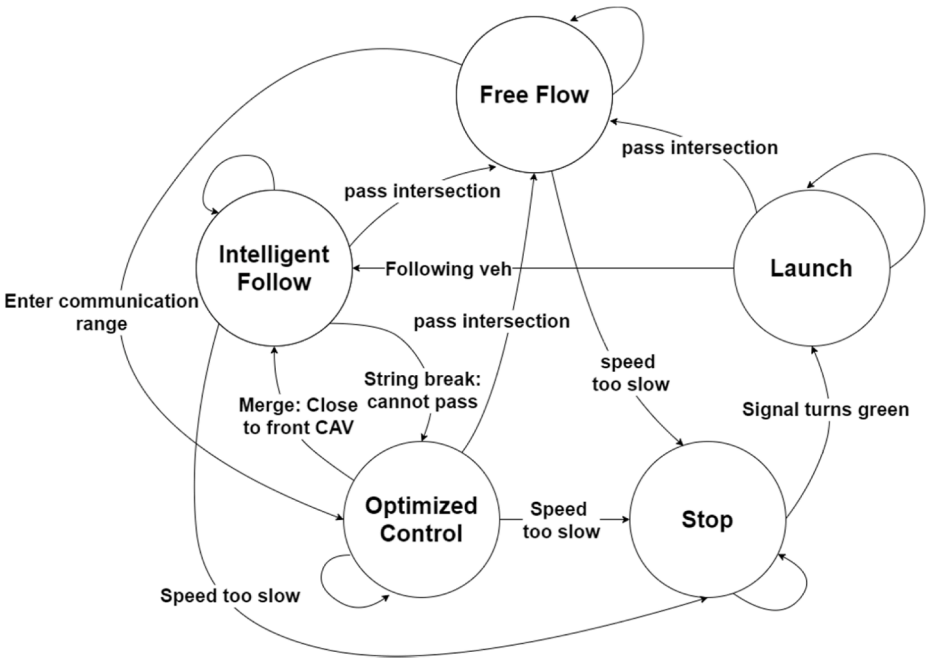

(a) State Transition Diagram

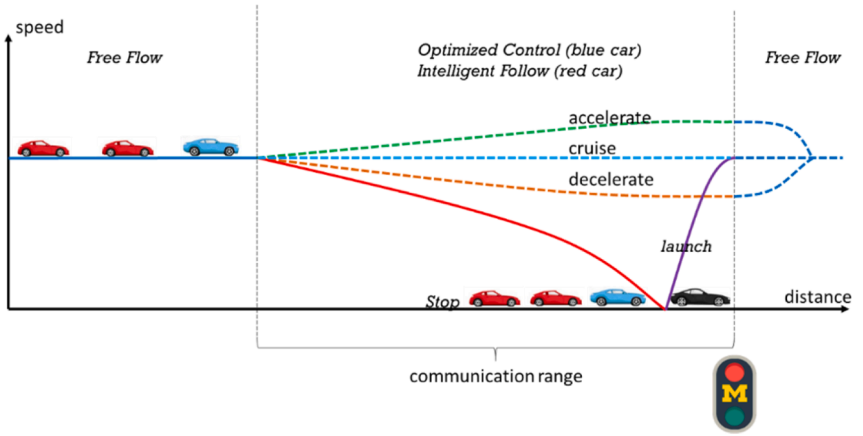

(b) CAV States and Operating Scenarios

Fig. 3. CAV Operating Scenarios and Transition Diagram.

cannot, it switches to the optimized control state to plan a stop speed profile. Consequently, the original platoon is split into two smaller platoons. In the optimized control state or launch state, if a CAV is approaching a leading CAV platoon, it will merge into the leading platoon and switch to the intelligent follow state if the distance is smaller than a threshold (e.g., 30 m).

Next, we introduce the vehicle models in each state.

In the free flow state and launch states, the vehicle is controlled by an Adaptive Cruise Control (ACC) algorithm, which applies the Intelligent Driver Model (IDM) (Kesting et al., 2010), shown in Eqs. (1) and (2). The reference acceleration is determined by the distance to the front vehicle and the current speed of the CAV. In the equations, Δd is the distance to the front vehicle and d_{min} represents the minimum safety distance.v^* is the desired speed and a^{ref} is the desired acceleration. δ is a model parameter that usually is set to 4.

$$a^{ref} = a^{+}_{max}\left(1 - \left(\frac{v}{v^*}\right)^{\delta} - \left(\frac{d^*}{\Delta d}\right)^2\right) \tag{1}$$

$$d^* = d_{min} + vh_{ref} + \frac{v\left(v - \widetilde{v}\right)}{2\sqrt{a^{+}_{max}a^{-}_{comfort}}} \tag{2}$$

In the intelligent follow state, the CAV is a following member of a CACC platoon. The acceleration of the CAV a^{ref} is calculated by a CACC model in (Van Arem et al., 2006), shown in Eq. (3), where a^{ref_v} is the reference acceleration based on the speed difference and a^{ref_d} is the reference acceleration based on the distance difference, calculated in Eqs. (4) and (5) respectively. d_{CACC} is the reference distance between two CACC vehicles. Note that in this model, "perfect following" is assumed, which ignores communication delay and string instability. The simplification is made for simulation of a large network. Readers can refer to (Feng et al., 2019; Feng et al., 2019; Li et al., 2015) for more detailed CACC models.

$$a^{ref} = min(a^{ref\_v}, a^{ref\_d}) \tag{3}$$

$$a^{ref\_v} = k(v^* - v) \tag{4}$$

$$a^{ref\_d} = k_a\widetilde{a} + k_v(\widetilde{v} - v) + k_d(\Delta d - d_{CACC}) \tag{5}$$

3.2. CACC leading vehicle trajectory planning

In the optimized control state, a trigonometric eco speed profile is generated for CACC leading vehicles. Note that a CACC platoon can consist of only one CAV. Based on the received time of arrival from the intersection controller, one of the four scenarios, shown in Fig. 2(a) will be chosen. More details on how to choose the scenarios can be found in our previous study (Yang et al., 2019). Except for the cruise scenario, speed profiles of the other three scenarios follow the trigonometric form, from which analytical solutions can be derived. Collision avoidance is added to the optimized control state that when the front vehicle of a CAV is an RV or CV and the car-following distance is small (e.g. an RV makes a cut-in in front of the subject CAV), the planned eco-trajectory is interrupted, and the CAV applies the IDM, to plan its trajectory to avoid collisions. That means the CAV chooses a more conservative acceleration between the planned eco-trajectory and the IDM.

The original trigonometric eco-trajectory planning model is proposed by (Barth et al., 2011), which generates a smooth vehicle trajectory giving terminal time (i.e., time of arrival at the intersection) to reduce fuel consumption and emissions. The terminal time (t_{arr}) is bounded by a green window, which defines the earliest and latest time the vehicle can arrive at the intersection, based on signal status and queue discharge time (Yang et al., 2019). In this work, initial acceleration is considered, which is always assumed to be zero in the original algorithm. This original algorithm works when the CAV is cruising towards an intersection at a constant speed. However, if the trajectory planning is executed when the CAV is accelerating or decelerating or the trajectory needs to be re-planned because of an updated green window, the zero initial acceleration setting will lead to a discontinuity in the acceleration profile. To address this issue, a new segment of the trigonometric profile $v_1(t)$ is added to first bring the acceleration back to 0. Then the eco planning algorithm is applied, as shown in Eqs. (6)–(11).

$$v_1(t) = \frac{a_0^2}{jerk_{max}}\sin\left(\frac{jerk_{max}}{a_0}t\right) + v_{init}\ , t \in [0, t_o) \tag{6}$$

$$v_2(t) = \begin{cases} v_p - v_r\cos(m(t - t_o)), t \in [t_o, t_p) \\ v_p - v_r\dfrac{m}{n}\cos\left[n\left(t - t_o + \dfrac{\pi}{2n} - t_p\right)\right], t \in [t_p, t_q) \\ v_p + v_r\dfrac{m}{n}, t \in [t_q, t_{arr}) \end{cases} \tag{7}$$

$$v_p = \frac{d^{stop} - \left(\frac{\pi a_0 v_{init}}{2jerk_{max}} + \frac{a_0^3}{jerk_{max}^2}\right)}{t^{arr} - t_o} \tag{8}$$

$$v_r = v_p - (v_{init} + \frac{a_0^2}{jerk_{max}}) \tag{9}$$

$$t_o = \frac{\pi a_0}{2 jerk_{max}}$$

$$t_p = t_o + \frac{\pi}{2m} \tag{10}$$

$$t_q = t_o + \frac{\pi}{2m} + \frac{\pi}{2n} \tag{11}$$

4. Intersection level models

The intersection controller is responsible for estimating and predicting traffic states, optimizing traffic signal parameters, and the time of arrival of CAVs. The methodology of traffic state estimation and prediction can be found in our previous work (Yang et al., 2019), which predicts the queuing dynamics with CV and/or loop-detector data, and estimates total vehicle delay using the shockwave profile model (Wu and Liu, 2011) and input and output model (Sharma et al., 2007). Each vehicle is first mapped at the lane level and sorted according to its estimated distance to the stop bar. The location and speed of each vehicle are obtained directly from the BSM if it is a CV or CAV, or estimated if it is an RV, which is introduced later in Eq. (13). After the localization, the traffic state estimation algorithm utilizes shockwave models to calculate current queue length and estimate the maximum queue length and discharge time of the queue based on signal information. The prediction results not only affect the number of vehicles that will be served during green interval for each approach, but also provide a green window to the CAVs, which serves as the lower and upper boundaries of the time of arrival assignments. The beginning of the green window for a CAV is defined as the time point when the CAV's front vehicle passes the intersection after the green start. The end of the green window is the same as the green end. With the estimated traffic state, a mixed-integer linear programming (MILP) problem is formulated in this section to jointly optimize traffic signal parameters and time of arrivals of CAVs.

The objective of the joint optimization is to minimize total delay and improve the efficiency of the intersection operation as shown in (12). $\lambda\delta_{\phi^*}$ in the objective is used as a soft constraint for dynamic offset allocation, which will be explained in the signal constraints. The decision variables include signal parameters and time of arrivals of each CAV at the intersection.

$$minimize \sum_j \sum_k \sum_s D_{jks} + \lambda\delta_{\phi^*} \tag{12}$$

$$s.t. D_{jks} = t_{jks}^{arr} - \frac{d_{jk1}^{stop} + (s-1)h_{CACC}v_{jk1}}{v_j^{max}}, \forall j, k, s$$

Signal constraints

Time of arrival constraints

CACC platoon split constraints

Where j is the lane index, and k is the vehicle group index in the lane. A vehicle group can be either a platoon of CAVs, an RV, a CV, or a

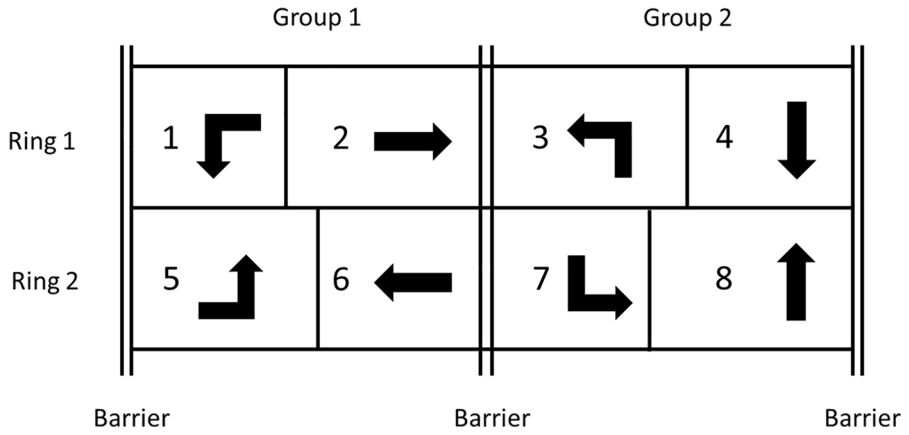

Fig. 4. NEMA Ring Barrier Structure of Signal Timing.

single CAV not in a platoon. s denotes the order of a vehicle in the vehicle group, and for a single-vehicle group, $s = 1$. h_{CACC} is the CACC headway. The first constraint shows that the delay of each vehicle is equal to the total travel time minus free-flow travel time to the intersection. Notice that for the following vehicles in a CAV platoon, their free-flow travel time can be calculated based on the free-flow travel time of the leading vehicle plus the CACC headway. Other constraints include traffic signal constraints for the dual-ring barrier controller structure, time of arrival constraints that determine whether a vehicle can pass the intersection during the current cycle or next cycle, and CACC platoon split constraints that determine whether a CAV platoon should split or not. Before we introduce the details of the constraints, the estimation of d_{jks}^{stop} and v_{jks} is presented.

CVs and CAVs broadcast BSMs, which include accurate location and speed information (i.e. d_{jks}^{stop} and v_{jks}) at each time step. For RVs, their locations and speeds are recorded by the entrance loop detector when they enter the link. After RVs pass the loop detector, Eq. (13) is used to estimate the locations and speeds at each time step, assuming that the RVs are traveling with the speed limit v_{jks}^{max}. Where, d_j^{detect} denotes the distance from the detector to the stop bar of lane j.

$$d_{jks}^{stop} = \max(d_j^{detect} - v_{jks}^{max}\Delta t_{jks}^{detect}, 0) \tag{13}$$

4.1. Signal constraints

Signal constraints mainly represent the standard NEMA dual-ring barrier structure, as shown in Fig. 4.

Eqs. (14)–(18) show the signal constraints, in which θ_ϕ is the green split of phase ϕ and C is a common cycle length. The intersections in the corridor are divided into a master intersection and other intersections. The master intersection applies Eqs. (14)–(17), where the cycle length is fixed and the reference point (i.e. start of the coordinated phase) does not change. Other intersections adopt Eqs. (15)–(18), in which their reference points are adjusted based on the optimized offset from the corridor coordinator. In this way, the cycle lengths of such intersections are dynamically adjusted as well, according to the assigned offsets. To better illustrate the idea, an example of the signal timing of the coordinated phase is shown in Fig. 5. The cycle length of the master intersection is 100 s in this example. The coordinated phase of intersection 2 starts 3 s later than the coordinated phase of the master intersection, so initially, the offset is 3 s. After the optimization of the offset, the new optimized offset becomes 5 s, so the reference point of intersection 2 is adjusted accordingly. In this way, the cycle length of intersection 2 extends to 102 s. Note that since the offset adjustment is small, the transition between different offsets is done within one cycle by adjusting the green split of other phases. By varying the offset and cycle length accordingly, different platoon sizes and platoon arrival times are accommodated.

A lane-to-phase mapping function $\phi = f(j)$ maps the lane index to 8 phases in the dual-ring structure. g_ϕ^{elps} denotes the elapsed green time of phase ϕ, and if phaseϕ is red, $g_\phi^{elps} = 0$. t_ϕ^{lost} denotes the lost time of all phases, including the duration of the yellow interval and all-red interval. I_ϕ^g is a binary variable, which equals to 1 if phase ϕ is green, and 0 otherwise. Eq. (14) shows that the summation of the green splits in each ring should be equal to the cycle length C at the master intersection. For each barrier, the summation of the green splits of ring 1 should be equal to the summation of the green splits of ring 2 (Eq. (15)). Eq. (16) shows that when phase ϕ is green, the summation of the remaining green timeg_ϕ^{rem}, the elapsed time g_ϕ^{elps}, and the lost time t_ϕ^{lost}should be equal to the green splitθ_ϕ. In addition, the remaining red time of phase ϕ, r_ϕ^{rem} is 0. When phase ϕ is red, the remaining green time g_ϕ^{rem} is equal to 0, and the remaining red time r_ϕ^{rem} should be equal to the summation of the remaining green time $g_{\widetilde{\phi}}^{rem}$ of the current green phase $\widetilde{\phi}$, the lost time $t_{\widetilde{\phi}}^{lost}$, and the summation of the green split $\sum_{\overline{\phi}}\theta_{\overline{\phi}}$of phases after $\widetilde{\phi}$ and before ϕ (Eq. (17)). $\overline{\phi}$ denotes the phase(s) that turns to green before phase ϕ in the same cycle.

To accommodate varying traffic demands from the side street and upstream intersection, the offset is not fixed. With the offset received from the corridor-level coordinator, Eq. (18) determines the start time of the coordinated phase, which is the reference point. Taking intersection i as an example, the green start of one coordinated phase of the next cycle should be equal to the offset between intersection $i-1$ to intersection i (i.e. $\xi_{i-1,i}$) plus the green start of the coordinated phase of intersection $i-1$ (i.e. $t_{(i-1)\phi^*}^{start}$). $\sum_{\overline{\phi}^*}\theta_{\overline{i\phi}^*}$ is the

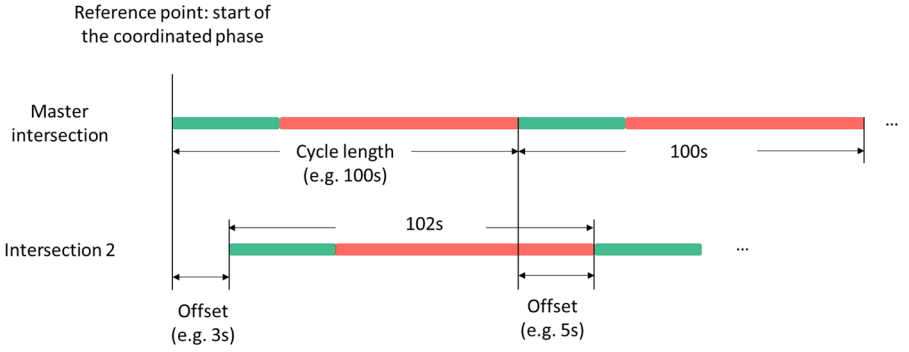

Fig. 5. Signal Timing of the Coordinated Phase.

summation of the green split from the next phase until the coordinated phase. An adjustment bound δ is added in the objective function as a soft constraint (i.e., $\lambda\delta_{i_x\phi^*}$). As a result, the start of the coordinated phase can vary within the bound to guarantee the feasibility.

$$\sum_{\gamma}\sum_{\sigma}\theta_{\phi_{1\gamma\sigma}} = \sum_{\gamma}\sum_{\sigma}\theta_{\phi_{2\gamma\sigma}} = C \tag{14}$$

$$\sum_{\sigma}\theta_{\phi_{1\gamma\sigma}} = \sum_{\sigma}\theta_{\phi_{2\gamma\sigma}}, \gamma = 1, 2. \tag{15}$$

$$g_{\phi}^{rem} = \begin{cases} \theta_{\phi} - (g_{\phi}^{elps} + t_{\phi}^{lost}), I_{\phi}^{g} = 1 \\ 0, otherwise \end{cases}, \forall \phi, \tag{16}$$

$$r_{\phi}^{rem} = \begin{cases} g_{\phi}^{rem} + t_{\phi}^{lost} + \sum_{\overline{\phi}}\theta_{\overline{\phi}}, I_{\phi}^{g} = 0 \\ 0, otherwise \end{cases}, \forall \phi \tag{17}$$

$$\xi_{i-1,i} + t_{(i-1)\phi^*}^{start} - \delta_{i\phi^*} \le g_{i\phi}^{rem} + t_{i\phi}^{lost} + \sum_{\vec{\phi}^*}\theta_{i\vec{\phi}^*} \le \xi_{i-1,i} + t_{(i-1)\phi^*}^{start} + \delta_{i\phi^*}, I_{\phi^*}^{g} = 0. \tag{18}$$

4.2. Time of arrival constraints

The time of arrival constraints are mainly used to determine whether a vehicle can pass the intersection during the current cycle or the next cycle, assuming the intersection is not oversaturated. The details of the constraints are shown in Eqs. (19)–(26). Two binary variables, $u_{jks}^{g}$and u_{jks}^{r}, are introduced for different phase states. $u_{jks}^{g} = 1$, when the current phase of lane j is green, and the vehicle can pass the intersection during the cycle, and 0 otherwise. $u_{jks}^{r} = 1$, when the current phase of lane j is red, and the vehicle can pass the intersection during the upcoming green phase, and 0 otherwise. Notice that the constraints with u_{jks}^{g} (Eqs. (19) and (20)) are only valid when the phase of lane j is green (i.e. $I_{f(j)}^{g} = 1$), and the constraints with u_{jks}^{r} (Eqs. (21) and (22)) are only valid when the phase of lane$j$ is red (i.e. $I_{f(j)}^{g} = 0$).

When the signal is green, if the time of arrival of the vehicle t_{jks}^{arr} is less than the remaining time of the current green phase, the vehicle can pass the intersection during the current green phase. Otherwise, the time of arrival should be greater than the summation of the remaining green time $g_{f(j)}^{rem}$, the red duration of other phases, and the discharge time of the queue t_{jks}^{leave}. Similarly, when the signal is red, if the time of arrival t_{jks}^{arr} is less than $r_{f(j)}^{rem} + \theta_{f(j)}$, the vehicle can pass the intersection during the next green phase, and the arrival time should be greater than $r_{f(j)}^{rem} + t_{jks}^{leave}$ (Eq. (23)). Otherwise, the vehicle has to wait for another cycle. It is assumed that the traffic demand is under-saturated and no vehicle has to stop twice at an intersection (i.e., the arrival time should be less than $r_{f(j)}^{rem} + C$). Eq. (24) shows that the arrival time of a group leading vehicle (either CACC platoon leading vehicle or RV/CV) should be greater than the free-flow travel time, and Eq. (25) shows that the arrival time of the group leading vehicle should be greater than the arrival time of its front vehicle $t_{j(k-1)N_{j(k-1)}}^{arr}$ plus the RV headway h_{RV}. Eq. (26) shows that the discharge time of the queue t_{jks}^{leave} should be equal to the number of vehicles in the queue times the headway (h_{RV} *or* h_{CACC}).

$$M\left(1 - u_{jks}^{g}\right) \ge I_{f(j)}^{g}\left(t_{jks}^{arr} - g_{f(j)}^{rem}\right) \ge -Mu_{jks}^{g}, u_{jks}^{g}\text{binary} \tag{19}$$

$$Mu_{jks}^{g} \ge I_{f(j)}^{g}(g_{f(j)}^{rem} + \left(C - \theta_{f(j)}\right) + t_{jks}^{leave} - t_{jks}^{arr}) \ge -M\left(1 - u_{jks}^{g}\right) \tag{20}$$

$$M\left(1 - u_{jks}^{r}\right) \ge \left(1 - I_{f(j)}^{g}\right)\left(t_{jks}^{arr} - r_{f(j)}^{rem} - C\right) \ge -Mu_{jks}^{r}, u_{jks}^{r}\text{binary} \tag{21}$$

$$Mu_{jks}^{r} \ge \left(1 - I_{f(j)}^{g}\right)\left(r_{f(j)}^{rem} + \theta_{f(j)} - t_{jks}^{arr}\right) \ge -M\left(1 - u_{jks}^{r}\right) \tag{22}$$

$$t_{jks}^{arr} \ge (r_{f(j)}^{rem} + t_{jks}^{leave})(1 - I_{f(j)}^{g}) \tag{23}$$

$$t_{jk1}^{arr} \ge \frac{d_{jk1}^{stop}}{v_{ij}^{max}} \tag{24}$$

$$t_{jk1}^{arr} \ge t_{j(k-1)N_{j(k-1)}}^{arr} + h_{RV}, \forall k > 1 \tag{25}$$

$$t_{jks}^{leave} = \left(1 - I_{f(j)}^{g}\right)\left(kh_{RV}u_{jkN_{jk}}^{r} + \sum_{k' \le k} \sum_{s < N_{jk}} h_{CACC} u_{jk's}^{r}\right) + I_{f(j)}^{g}\left(kh_{RV}\left(1 - u_{jkN_{jk}}^{g}\right) + \sum_{k' \le k} \sum_{s < N_{jk}} h_{CACC}\left(1 - u_{jk's}^{g}\right)\right) \tag{26}$$

4.3. CACC platoon split constraints

CACC platoon split constraints determine whether a CACC platoon needs to split or not based on the remaining green time, shown in Eqs. (27) and (28). When the signal is green ($I_{f(j)}^{g} = 1$) and all CAVs in the platoon can pass the intersection during the current green phase ($u_{jks}^{g} = 1$), the platoon does not split and $t_{jks}^{arr} = t_{jk(s-1)}^{arr} + h_{CACC}$. Otherwise, the string splits and based on Eq. (20), the new platoon's arrival time should fulfill $t_{jks}^{arr} \ge g_{f(j)}^{rem} + \left(C - \theta_{f(j)}\right) + t_{jks}^{leave}$. Similarly, when the signal is red ($I_{f(j)}^{g} = 0$), if all the CAVs in the platoon can pass the intersection during the upcoming green phase ($u_{jks}^{r} = 1$), then the platoon does not split, and $t_{jks}^{arr} = t_{jk(s-1)}^{arr} + h_{CACC}$. Otherwise, the platoon splits and based on Eq. (23), the new platoon's arrival time should fulfill $t_{jks}^{arr} \ge r_{f(j)}^{rem} + t_{jks}^{leave}$. Eq. (28) shows that for the platoon leading CAV, the arrival time should be greater than the earliest arrival time given the acceleration/deceleration, and jerk limits in the trigonometric eco-trajectory planning.

$$t_{jk(s-1)}^{arr} + h_{CACC} + I_{f(j)}^{g} M\left(1 - u_{jks}^{g}\right) + \left(1 - I_{f(j)}^{g}\right) M\left(1 - u_{jks}^{r}\right) \ge t_{jks}^{arr} \ge t_{jk(s-1)}^{arr} + h_{CACC} - I_{f(j)}^{g} M\left(1 - u_{jks}^{g}\right) - \left(1 - I_{f(j)}^{g}\right) M\left(1 - u_{jks}^{r}\right), s > 1 \tag{27}$$

$$t_{jk1}^{e} - \left(1 - I_{jk}^{CACC}\right) M \le t_{jk1}^{arr} \tag{28}$$

After the optimization is executed, the arrival time of each platoon leading CAV and whether the platoon needs to split are sent to the vehicle level. If the platoon does not split, the leading vehicle follows the optimized arrival time to generate its speed profile (Section 3.2), and the following vehicles stay in the intelligent follow state with the desired CACC headway. If the platoon needs to split, the vehicle at the split position receives its new time of arrival from the intersection controller. This vehicle serves as the leading CAV of a new platoon and switches the state to optimized control. It then generates a new speed profile based on the assigned arrival time.

5. Corridor level models

The corridor coordinator determines the offsets for the coordinated phases of each intersection, promoting two-way coordination. To reduce the computational burden, all vehicles in the coordinated phase are considered as one platoon and a link performance function is proposed to calculate the total delay of the vehicles in the platoon. The link performance function was first introduced in (Gartner et al., 1975), but was utilized offline, without the consideration of vehicle arriving from the side street. In (Beak et al., 2017), Beak et al. implemented the link performance function in a real-time fashion. However, only one-way coordination was considered, which makes the problem much easier. In this paper, two-way real-time coordination is proposed using the link performance function.

Fig. 6 illustrates a three-intersection corridor with two-way coordination, and we take the eastbound through movement of intersection i as an example to introduce two types of platoons for the coordinated phase. The secondary platoon, denoted by a yellow rectangle, consists of vehicles from the side streets of the upstream intersection $i-1$. The number of vehicles in the secondary platoon is calculated by the turning ratio and volume from the side street of intersection $i-1$. The primary platoon (the blue rectangle) consists of the vehicles from the coordinated phase of the upstream intersection $i-1$. When the signal of the coordinated phase at intersection $i-1$ is red, the number of vehicles in the primary platoon $\Psi_{i\phi^*}$ of intersection i can be estimated by Eq. (29), which is the summation of the current queue length ($q_{(i-1)\phi^*}$) and the estimated arriving vehicles based on the average historical demand ($V_{(i-1)\phi^*}$) of the coordinated phase. When the signal of intersection $i-1$ is green, the primary platoon $\Psi_{i\phi^*}$ of intersection i can be estimated by Eq. (30), in which h'

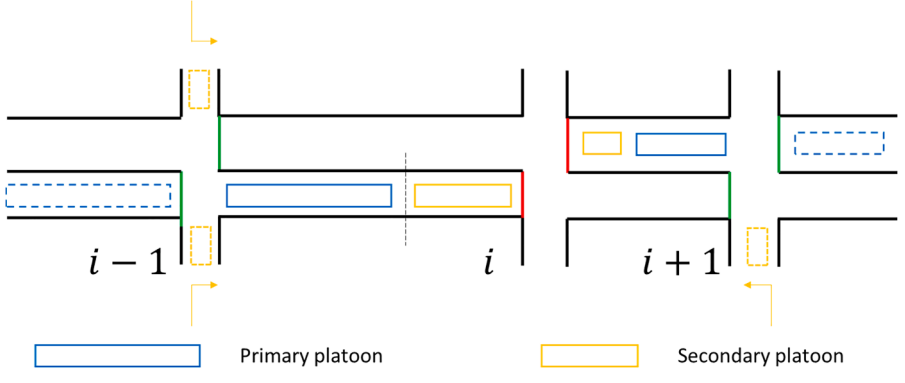

Fig. 6. Platoons for the Coordinated Phase.

is the estimated saturation headway. When the penetration rate of the CAV is low (i.e. $< 75\%$), we consider $h^{'} = h_{RV}$. Otherwise, we consider $h^{'} = h_{CACC}$ since CACC platoons are more likely to be generated. The primary platoon is estimated by the summation of the queue length at the start of the green $q^{'}_{(i-1)\phi^*}$ and the demand $V_{(i-1)\phi^*}$ times the remaining green time after the queue (i.e. $q^{'}_{(i-1)\phi^*}$) discharges (30). As a result, the link performance function of intersection i is the total delay of the primary and secondary platoons from intersection $i-1$. Note that right turning vehicles at intersection $i-1$ and left turning vehicles at intersection i are subtracted from the total number of vehicles when calculating $\Psi_{i\phi^*}$ in Eqs. (29) and (30). Fixed turning ratios (i.e. right turning ratio $\zeta_{(i-1)\phi^*}$ and left turning ratio $\xi_{i\phi^*}$), calibrated from the historical data, are assumed when estimating the lengths of primary and secondary platoons.

$$\Psi_{i\phi^*} = \begin{cases} (q_{(i-1)\phi^*} + \left(C - r^{elps}_{(i-1)\phi^*}\right)V_{(i-1)\phi^*})(1-\zeta_{(i-1)\phi^*})(1-\xi_{i\phi^*}), I^{g}_{\phi^*} = 0 & (29) \\ \left(q^{'}_{(i-1)\phi^*} + \left(\overline{g}_{(i-1)\phi^*} - q^{'}_{(i-1)\phi^*}h^{'}\right)V_{(i-1)\phi^*}\right)\left(1-\zeta_{(i-1)\phi^*}\right)(1-\xi_{i\phi^*}), otherwise & (30) \end{cases}$$

After the estimation of the platoon lengths, the link performance function is calculated as the total delay of the primary platoon. Notice that only delay from the primary platoon is considered because the main purpose of coordination is to enhance the progression of coordinated phases. Fig. 7 shows six different scenarios of link performance function calculation. In the figure, the notations are simplified, and the coordinated phase ϕ^* of the intersection i is used for illustration. Take the second case as an example, the x-axis represents time, and the y-axis denotes the number of vehicles arrived at the intersection. The zero point of the x-axis is moved to be the start of green for better illustration. Then $-r$ is the red start and g is the green end, which represent a whole cycle. e is the time point when the secondary platoon is fully discharged after the signal turns to green. The length of the primary platoon (black dashed rectangle) is represented in time, and its duration p is assumed to be equal to the green time of the coordinated phase of the upstream intersection. Based on the calculation of the number of vehicles in the primary platoon (Eqs. 29 and 30), the average headway h (height of the dashed rectangle) in the figure can be calculated as $h = \frac{\Psi}{p}$. After the first vehicle of the primary platoon arrives at the intersection

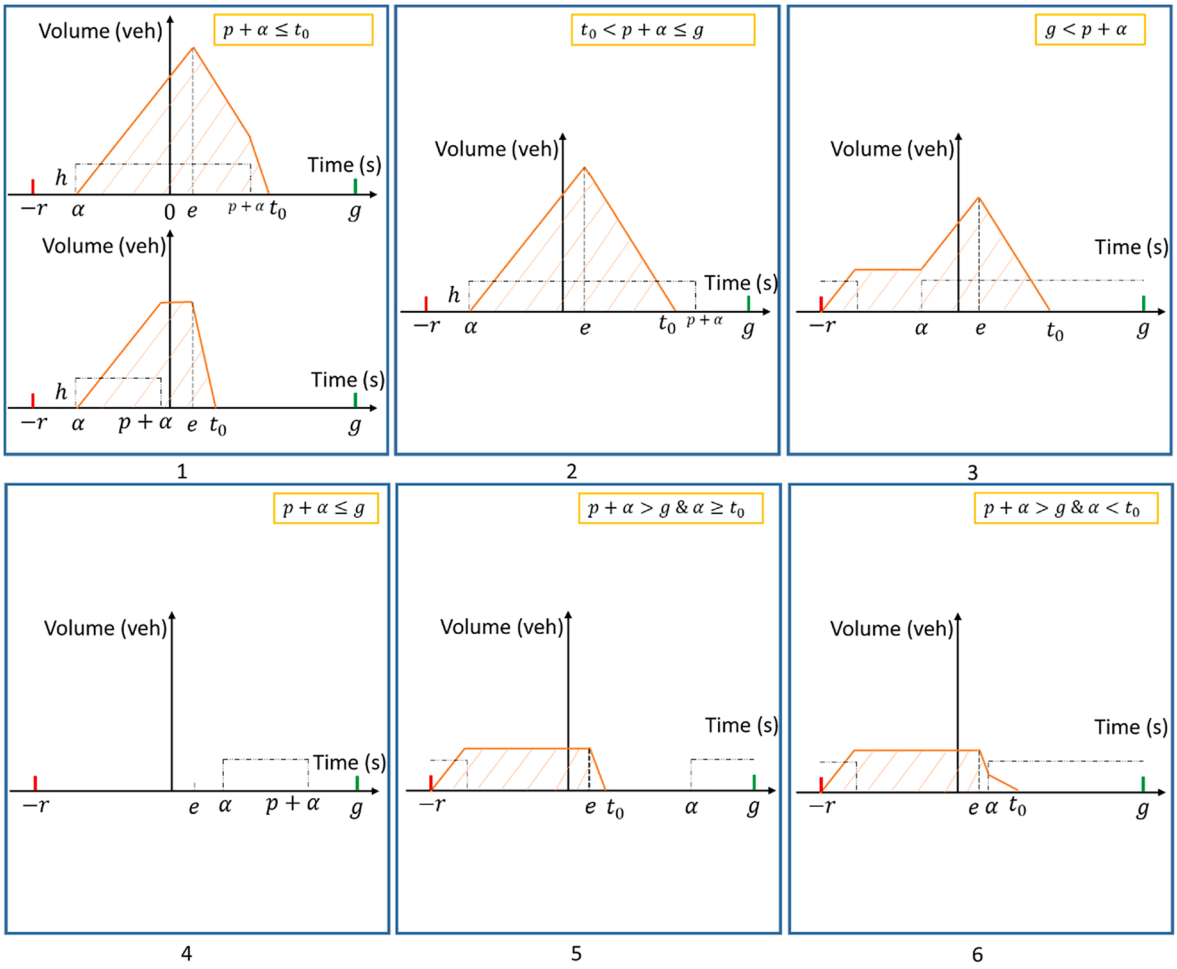

Fig. 7. Link Performance Function of Different Scenarios.

at time point α, the primary platoon starts to accumulate delays. After the secondary platoon is fully discharged, the primary platoon starts to discharge from the intersection with the saturation flow rate. At $t_0 = e + p \times \frac{h}{s}$, the entire queue at the intersection is fully discharged, so the vehicles in the primary platoon that arrives later than t_0 do not experience any delay. The total delay of the primary platoon in the coordinated phase can be represented by the shaded area.

In subfigures 1, 2 and 3, the arrival time of the primary platoon α is earlier than e. In subfigure 1, the last vehicle in the primary platoon arrives at the intersection earlier than the time point when the queue is fully discharged (i.e. $p + \alpha \le t_0$). Notice that although the shape of the shaded area in the two cases (i.e. $p + \alpha \le e, p + \alpha > e$) of subfigure 1 looks different, the link performance function is the same (LPF_1). In subfigure 2, the last vehicle arrives at the intersection later than t_0 but earlier than the end of the green, while in subfigure 3, part of the platoon arrives at the intersection after the end of the green (i.e. $p + \alpha > g$), which causes extra delay in the next cycle (i.e., delay starts to accumulate at $-r$). In subfigures 4, 5 and 6, the arrival time of the primary platoon α is later than e. In subfigure 4, the last vehicle arrives at the intersection earlier than the end of the green (i.e. $p + \alpha < g$), so no vehicle in the primary platoon experiences any delay. In subfigure 5 and 6, part of the platoon arrives at the intersection later than the end of the green, which causes extra delay, similar to subfigure 3. In subfigure 5, the first vehicle in the primary platoon arrives later than t_0, and in subfigure 6, the first vehicle arrives earlier than t_0. Based on the different situations, the link performance functions LPF_1 LPF_6 under different scenarios are shown in Eqs. (31)–(36).

$$LPF_1 = \frac{p^2 h(y-1)}{2} - ph(\alpha - e) \ , \alpha \le e \ and \ p + \alpha \le t_0 \tag{31}$$

$$LPF_2 = \frac{h(\alpha - e)^2}{2(1-y)} \ , \alpha \le e \ and \ t_0 < p + \alpha \le g \tag{32}$$

$$LPF_3 = (g + r - p)(p - g + \alpha)h + \frac{h(p - g + e)^2}{2(1-y)} \ , \alpha \le e \ and \ g < p + \alpha \tag{33}$$

$$LPF_4 = 0 \ , \alpha > e \ and \ p + \alpha \le g \tag{34}$$

$$LPF_5 = \frac{h(p - g + \alpha)^2 (y-1)}{2} + (\mathrm{p} - \mathrm{g} + \alpha)h(r + \alpha) \ , \alpha \ge t_0 \ and \ p + \alpha > g \tag{35}$$

$$LPF_6 = (g + r - p)(p - g + \alpha)h + \frac{h(p - g + e)^2}{2(1-y)} \ , e < \alpha < t_0 \ and \ p + \alpha > g \tag{36}$$

Notice that all the link performance functions are either linear or quadratic, it is easy to prove the convexity of the whole function. By aggregating the pieces of each link performance function ($LPF_1 \sim LPF_6$), we get a complete link performance function in terms of the arrival time of the first vehicle of the primary platoon (i.e. α), as shown in Fig. 8. In the left subfigure, the platoon length plus the discharge time of the secondary platoon e is less than the green split g. When α is between e and $g - p$, the vehicles in the primary platoon do not experience any delay. In the right subfigure, when $p + e > g$, the vehicles must experience some delay regardless of arrival time.

By replacing the quadratic function with its linear approximation, the whole link performance function can be expressed as a piecewise linear function. The mathematical optimization problem for the corridor-level coordinator is shown in (37). $\bar{g}_{i\phi^*}$ and $\bar{r}_{i\phi^*}$ denotes the average green duration and average red duration of coordinated phase ϕ^* of intersection i, based on the optimized green durations and red durations of all previous cycles from the intersection level. $t^{travel}_{i-1,i}$ is the free flow travel time from intersection $i-1$ to intersection i, which can be calibrated offline from the historical data. $\alpha_{i\phi^*}$ and $\xi_{i-1,i}$ are decision variables that denote the arrival time of the first vehicle in the primary platoon and the offset of the coordinated phase from intersection $i-1$ to intersection i, respectively. The objective is to minimize the delay of all the coordinated phases, which is estimated by the link performance functions in Fig. 7. To

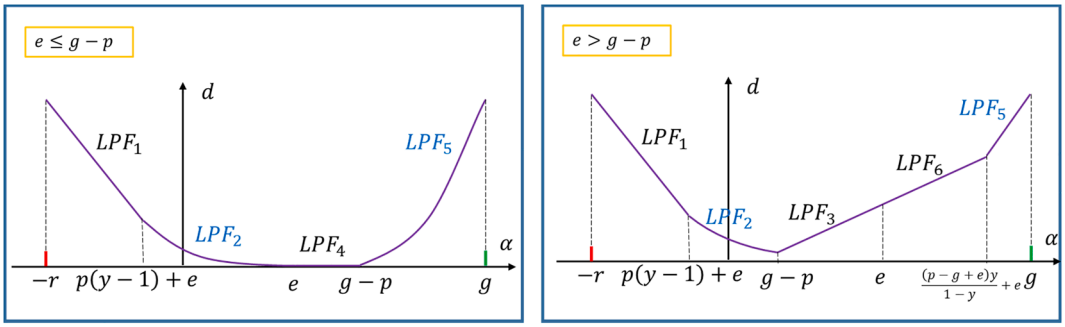

Fig. 8. Link Performance Function in terms of the Arrival Time of the First Vehicle.

formulate a convex optimization problem, the piecewise linear function can be represented by the constraints $\widetilde{D}_{i\phi^*} \geq LPF_w$ for each scenario w equivalently. The offset between intersection $i-1$ and intersection i is equal to the travel time on the link minus the arrival time. The arrival time should be between the start of the red and the end of green in each cycle. For two-way coordination,$\xi_{i-1,i} = -\xi_{i,i-1}$. Thus, the problem is formulated as a linear programming problem as shown in Eq. (37).

$$minimize \sum_i \sum_{\phi^*} \widetilde{D}_{i\phi^*} \tag{37}$$

$$s.t. \widetilde{D}_{i\phi^*} \geq LPF_w, \forall w$$

$$\xi_{i-1,i} = t_{i-1,i}^{travel} - \alpha_{i\phi^*}, \forall i$$

$$-\overline{r}_{i\phi^*} \leq \alpha_{i\phi^*} \leq \overline{g}_{i\phi^*}, \forall i$$

$$\xi_{i-1,i} = -\xi_{i,i-1}. i = 2 \cdots N$$

6. Numerical studies

6.1. Implementation procedure

Simulation experiments are conducted on a desktop with an Intel 3.4 GHz CPU with 4 cores and 16 GB memory. VISSIM is used as the simulation environment, which replaces the roadway component in Fig. 2. DriverModel.dll API (PTV, 2014) is used to implement the CAV trajectory planning models. The API is also used to generate BSMs for CAVs and RVs. When CAVs have to make a lane change to realize their predefined routes, VISSIM's internal lane-changing model is executed. In addition, virtual controllers in VISSIM are used to replace the real controllers in the intersection component. The overall simulation structure remains the same.

A flow chart of the simulation implementation is shown in Fig. 9. The purple blocks denote the CAV trajectory planning models, which generates CAV speed profiles and control the vehicles every 0.1 s. The green blocks denote the algorithms in the Intersection Controller module, which are executed every 3 s. A rolling horizon scheme is applied where the signal timing is generated for one cycle but only the first 3 s are implemented. The algorithms are written in C++ and Gurobi 8.1.0 (Optimization, 2014) is applied to solve both the MILP and LP problems. We use N_{veh} to denote the number of vehicles, N_{phase} to denote the number of phases, and $N_{platoon}$ to denote the number of platoons. In the MILP, the number of continuous variables is $2N_{veh} + 3N_{phase} + 2$, and the number of binary

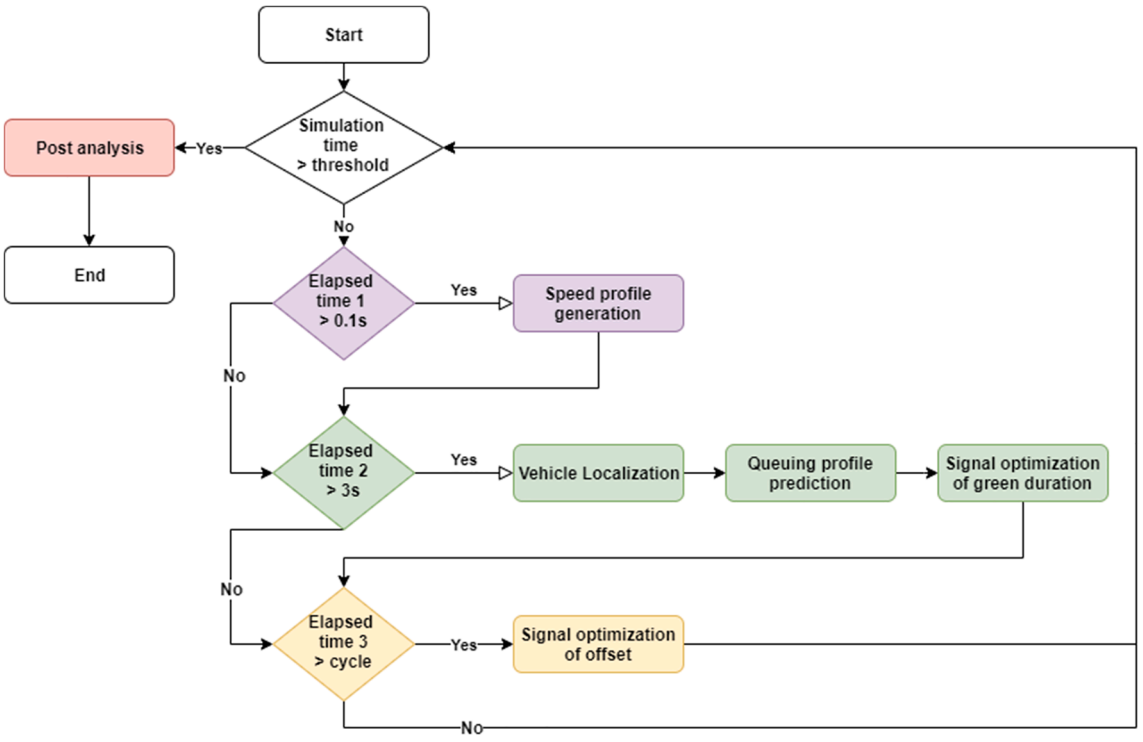

Fig. 9. Implementation Flow Chart.

variables is $2N_{veh}$. The number of integer variables is $2N_{platoon}$. The number of constraints is upper bounded by $9N_{veh} + 3N_{platoon} + 3N_{phase} + 4$, including $3N_{phase} + 4$ signal constraints, $7N_{veh} + 2N_{platoon}$ time of arrival constraints and $2N_{veh} + N_{platoon}$ CACC platooning constraints. Notice that $N_{platoon} = o(N_{veh})$, and the size of the problem is determined by traffic volume (i.e., N_{veh}) and CAV penetration rate (i.e., $N_{platoon}$). The MILP problem of the intersection level model can be solved within 0.1 s with 0.1% gap to the optimal solution under 100% CAV penetration rate. The yellow blocks denote the Corridor Coordinator model, which optimizes the offset every cycle. In the corridor level LP problem, there are $5N_{inter}$ continuous variables, where N_{inter} denotes the number of intersections in the system. The number of constraints is upper bounded by $8N_{inter}$. The problem can be solved within 0.01 s with 0.1% gap to the optimal solution.

6.2. Simulation experiments

A simulation model of the Plymouth Rd corridor, in Ann Arbor, Michigan is built in VISSIM (Fig. 10). The Plymouth corridor consists of six intersections, from Barton Dr. on the west to the Green Rd. on the east, which are indexed by $1 \sim 6$. The stretch of the Plymouth Rd is about 2.2 miles and has two lanes for each direction which is one of the busiest commuting routes, serving US23 to the North campus of the University of Michigan and downtown Ann Arbor. Some crossing roadways are major arterials that carry a large volume of traffic and others are side streets with less traffic demand. The volumes and turning ratios at each intersection in the simulation are calibrated with the real-world traffic data collected from afternoon peak hour (4:00 pm–5:00 pm). Coordinated actuated signal control is considered as the baseline for comparison, which is optimized by VISTRO (America, 2014). Fig. 11 shows the coordination diagram of the baseline signal control. The green shaded area denotes the green waves, which indicates good coordination patterns in both westbound (Fig. 11(a)) and eastbound (Fig. 11 (b)). The index of each intersection is shown at both sides of the figure for westbound and eastbound respectively. Notice that at least one stop is unavoidable due to two-way coordination.

Other critical parameters used in the simulation experiments are summarized in Table 2.

Two series of simulation experiments are conducted under different combinations of mixed traffic conditions. In the first series of experiments, there are only CV and CAV, with varying penetration rates of CAVs: 0%, 5%, 25%, 50%, 75%, and 100%. In the second series of experiments, all the CVs are replaced with RVs and the same set of CAVs penetration rates are considered. Notice that the first series has 100% connectivity, the main objective is to analyze the system performance under different levels of controllability by varying the penetration rate of the CAVs. In the second series, the connectivity is not 100% and the states of the RVs need to be estimated by loop detectors. Changing the penetration rate of the CAVs leads to the variations of both the controllability and the connectivity. The duration of each experiment is 2100 (sec) with 300 (sec) warm-up time, and each experiment is repeated with 5 random seeds. After each simulation run, all vehicle trajectories are recorded and sent to the post-analysis to calculate the fuel consumption and emissions by the MOVES model (Koupal et al., 2003). The experiment results are presented below.

Fig. 12 shows the simulation results at the network level, in which all vehicles in the simulation are taken into consideration. The left three subfigures ((a) – (c)) show the results of the first series of experiments (CAV + CV), while the right three subfigures ((d) – (f)) show the results of the second series of experiments (CAV + RV). For both series of experiments, with the increasing penetration rates of CAVs, the benefits from eco-trajectory planning are more significant. The average vehicle speed increases when there are more CAVs, because the eco-trajectory planning helps more CAVs pass the intersection without stop, also leading to the reduction of the number of stops. In terms of fuel consumption, since the speed profiles of the CAV are smoother and unnecessary acceleration and deceleration are avoided, the fuel consumption and emissions decrease as the penetration rate of CAV increases.

More detailed data can be found in Table 3. Note that the comparison between the baseline and 0% CAV shows the benefits of the corridor-level adaptive signal control, where no CAV time of arrival and trajectory are optimized. For the series with CVs, the total delay decreases by 14% (from 74.84 s to 64.40 s) and the fuel consumption decreases by 6.8% (from 4131KJ/mile to 3867KJ/mile) The results indicate that the performance can be improved greatly by CV based coordinated adaptive control. If the CVs are replaced by the

Fig. 10. Plymouth Corridor VISSIM Simulation Model.

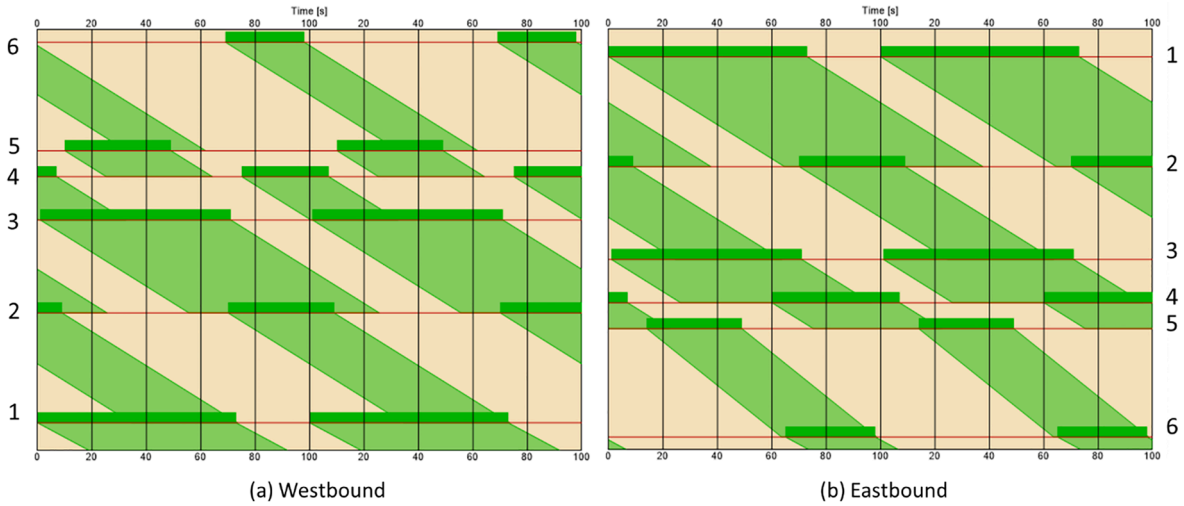

Fig. 11. Coordination Diagram of the Coordinated Actuated Signal Control (Baseline).

Table 2
Critical Parameters in Simulation Setup.

Parameter Name	Value
Speed Limit	35 mph on the west of Huron Road and 45 mph on the east of the Huron Road
Minimum Green Time	5 s
Maximum Green Time	100 s
Yellow Interval	4 s
All-red Clearance Interval	2 s
Gap out Time (in actuated control)	3 s
CACC headway (h_{CACC})	0.9 s
RV/CV headway (h_{RV})	1.8 s

RVs (series II), the total delay decreases by 0.6% (from 74.84 s to 74.39 s) and the number of stops decreases by 1.9%. The fuel consumption decreases by 3.8% (from 4131KJ/mile to 3972KJ/mile). The results indicate that even loop-detector based coordinated adaptive control outperforms the coordinated actuated control (baseline), but the improvement is not as significant as CV based coordinated adaptive control. When the penetration rate of the CAV is 100%, the delay further decreases by 33.0% (to 49.99 s) and fuel consumption decreases by 7.4% (to 3824KJ/mile) by comparing to the baseline because the CACC platoon has much shorter headways.

Comparing the second series of experiments with the first series, the high penetration rate of CAV leads to lower benefits in the second series in all performance indexes. The reason for this phenomenon is that the states of RVs are estimated from loop-detector data, which is not as accurate as the BSMs broadcast from the CVs. Therefore, the errors in traffic state estimation lead to suboptimal solutions in the signal optimization. Meanwhile, the inaccurate estimation of queuing dynamics also causes inaccurate time of arrivals for the CAVs and further influences the eco-trajectory planning. If the generated time of arrival is later than the optimal time of arrival, the green time is not fully utilized. On the other hand, the CAV's planned trajectory may be interrupted by its leading vehicle, which results in more fuel consumption and emissions.

Fig. 13 shows the simulation results of the mobility performance of two intersections. Most intersections have similar performances as the intersection of Green Rd. (subfigure b and d). When the penetration rate of CAV increases, the mobility improves in terms of the total vehicle delay, total stop delay, and the number of stops. At the intersection of Traverwood Dr. (subfigure a and c), mobility is getting worse when the penetration rate of CAV is low. However, since this is a T-intersection, and the demand for this intersection is not high, the total delay and the number of stops is much less than other intersections, so the performance doesn't impact the entire network a lot.

6.3. Sensitivity analysis

One feature of the proposed framework is that at the corridor level, the offset of each intersection is optimized each cycle to accommodate volume fluctuations. A series of sensitivity analysis is performed to further analyze the impact of dynamic offset optimization.

In the sensitivity analysis, the simulation period is divided into three intervals (300–900 s, 900–1500 s, 1500–2100 s), plus the warm-up time. In the second interval (900 – 1500 s), the traffic volume of the whole network is increased by 0%, 5%, or 10%. The traffic volumes of the first and third intervals remain unchanged. To analyze the benefits from the dynamic offset optimization, the

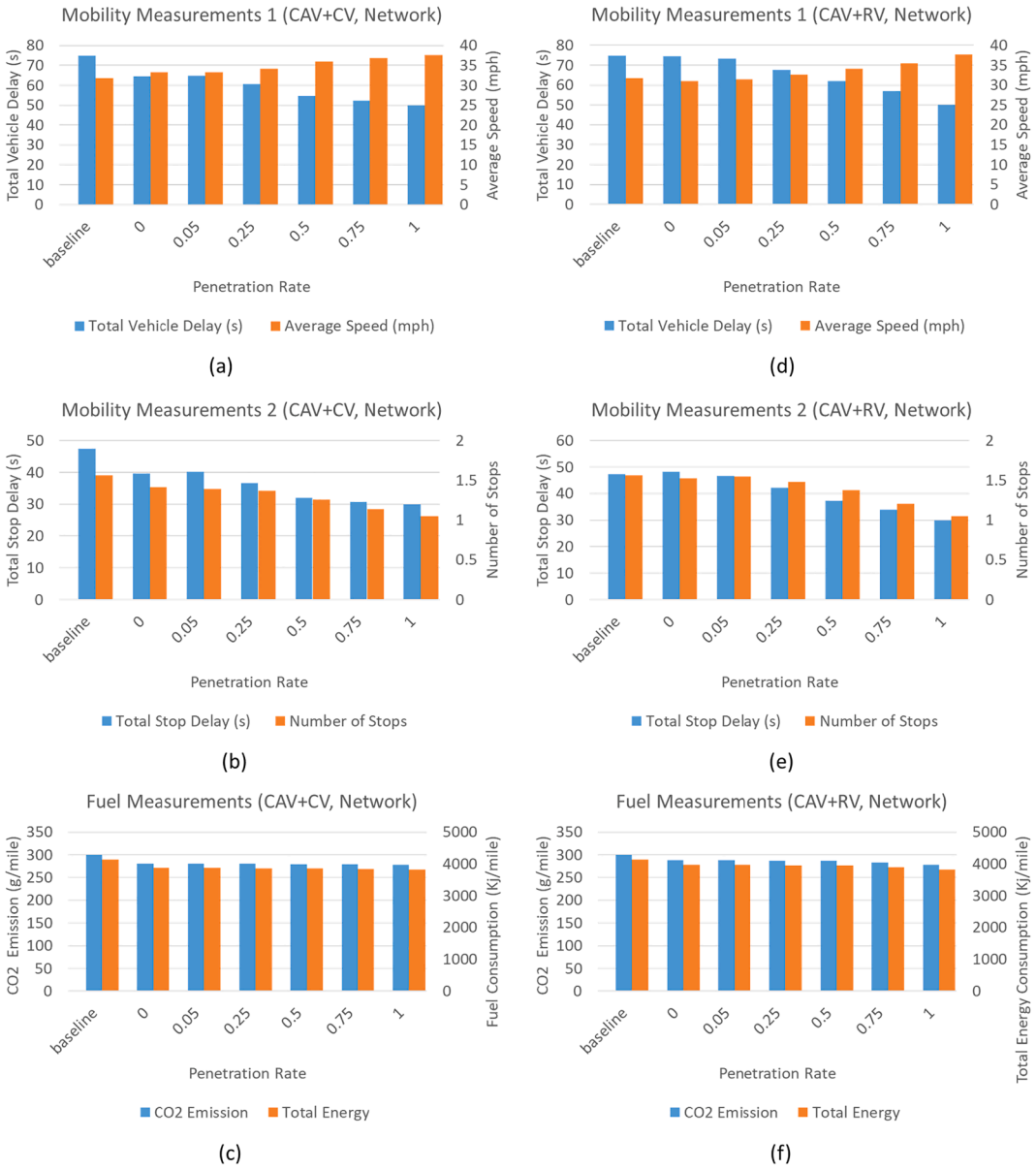

Fig. 12. Simulation Results of Network Level.

Table 3
Mobility and Fuel Measurements in Network Level.

Penetration rate		baseline	0	0.05	0.25	0.5	0.75	1
Delay (s)	CAV + CV	74.84	64.40	64.65	60.66	54.67	52.14	49.99
	CAV + RV	74.84	74.39	73.18	67.51	61.92	56.90	49.99
Number of stops	CAV + CV	1.56	1.42	1.39	1.37	1.26	1.14	1.05
	CAV + RV	1.56	1.53	1.55	1.48	1.37	1.20	1.05
Fuel consumption (KJ/mile)	CAV + CV	4131	3867	3868	3860	3852	3837	3824
	CAV + RV	4131	3972	3969	3951	3950	3898	3824

baseline experiments use a fixed offset optimized by VISTRO in the corridor level model, and the intersection level model remains the same. All the vehicles in the sensitivity analysis are CVs, so that vehicle trajectories are not optimized.

Fig. 14 shows the improvement of dynamic offset optimization in terms of mobility and fuel economy, comparing to the baseline. The x-axis denotes the volume fluctuation percentage described above, and the y-axis denotes the percentage of improvement. It can be

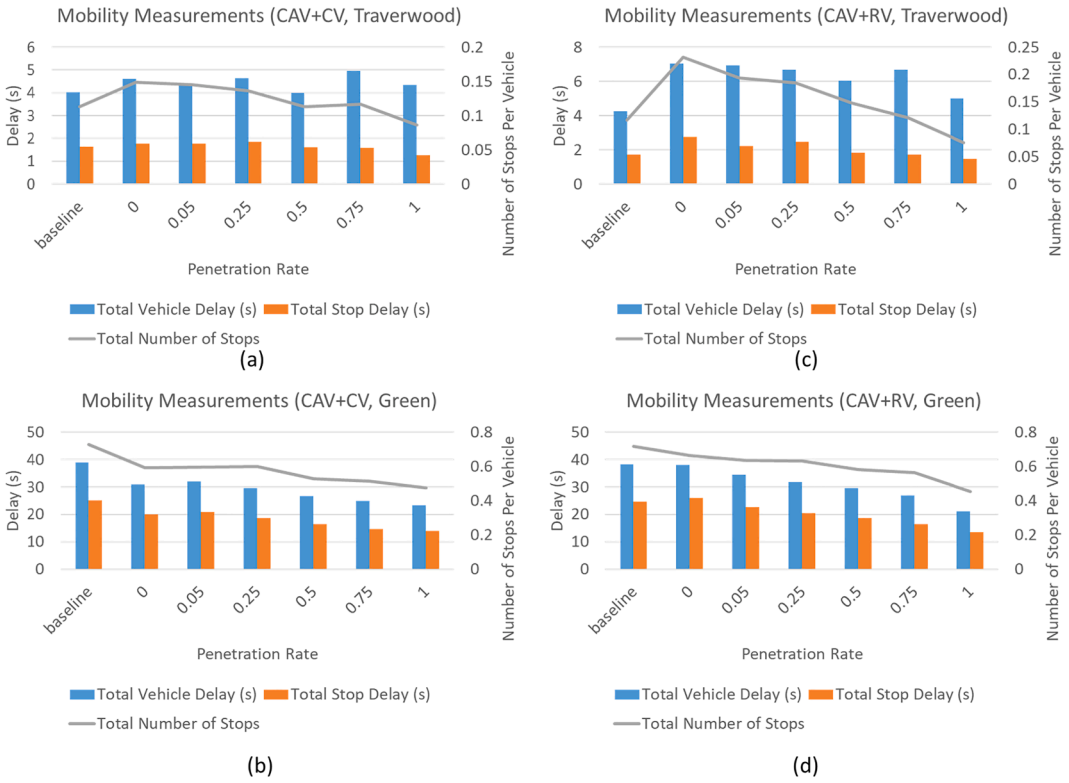

Fig. 13. Mobility Results of Intersection Level.

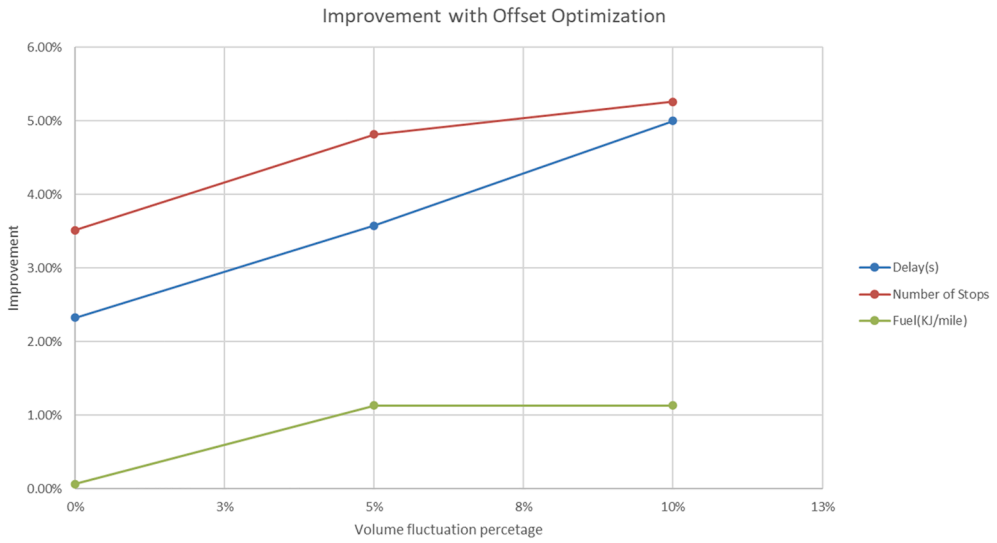

Fig. 14. Improvement with Offset Optimization.

seen from the figure that the benefits of dynamic offset optimization increase with higher volume fluctuations. When the volume fluctuation is 10%, the dynamic offset optimization further reduces 5.3%, 5.0% and 1.1% of the number of stops, delays and fuel consumption respectively, comparing to the baseline with fixed offsets.

Fig. 15 shows the offset variations of each intersection cycle by cycle. The dashed lines denote the baseline fixed offsets, and the solid lines with circles are the optimized offsets. Comparing to intersection 5 and 6, the offset of the first four intersections does not change a lot. In other words, for these four intersections, the coordination is always good. This can also be validated from the coordination diagram as shown in Fig. 11. Notice that the coordination between the fourth and the fifth intersection is sacrificed, for

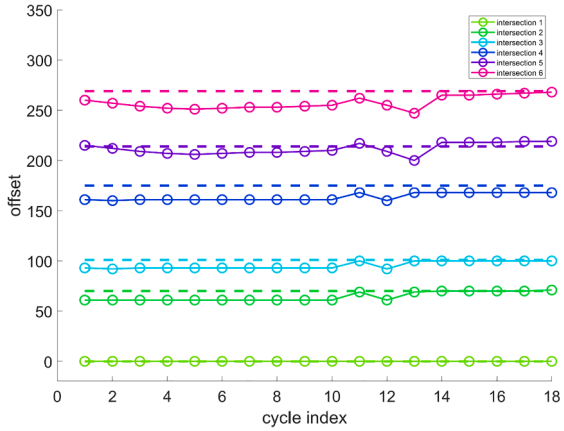

Fig. 15. Offset Variations at Different Intersections.

accommodating the coordination between other intersections. Thus, the variation of intersection 5 does not affect intersection 4 much. For intersections 5 and 6, when the volume does not fluctuate during the first interval (cycles 1–6), the offsets decrease and increase in the same trend. Although the volume starts fluctuating at cycle 7, the whole network has not been influenced by the volume fluctuation a lot and the offset between intersection 5 and 6 remains 45 s. The offset starts changing after several cycles, which keeps increasing to 49 s because the travel time becomes longer due to the larger volume. The additional mobility and fuel benefits through offset optimization in Fig. 15 mainly come from intersections 5 and 6, since they are the major intersections in the corridor and carry large volumes.

7. Conclusions and further research

This paper proposes a cooperative driving framework for arterial corridors in a mixed traffic condition of RV, CV, and CAV. In the vehicle level models, a state transition diagram is designed to accommodate different CAV maneuvers under different operating scenarios. A trigonometric speed profile is applied for eco-trajectory planning with consideration of non-zero initial accelerations. In the intersection level model, a MILP problem is formulated to optimize traffic signals and CAV time of arrivals with the objective of minimizing total delay, given the offset from the corridor coordinator. In the corridor level model, the link performance function is adopted to calculate the total delay of the coordinated phases. Link performance functions are derived under different arrival patterns to estimate the vehicle delay. With the approximation to piecewise linear link performance functions, the offset optimization problem can be formulated as an LP problem, which is easy to solve. Simulation experiments of an arterial corridor have been performed, using real-world traffic data. Results show that the total delay decreases by 14% and the fuel consumption decreases by 6.8% due to CV-based coordinated adaptive control with dynamic offsets. When the CAV comes into play, the total delay and fuel consumption further decrease as the penetration rates of the CAV increase. When the penetration rate of CAVs is 100%, the total delay and fuel consumption reduction raises to 33% and 7.4% respectively. A sensitivity analysis of volume fluctuation has been conducted, which shows the benefits of the dynamic offset optimization at the corridor level.

In future work, the lateral behavior of CAVs needs to be explicitly modeled for the cooperation between CAVs in different lanes in the vehicle level model. The optimization at the intersection level not only provides the time of arrival of the CAVs as the guidance but may also provide lane change guidance (e.g., lane change location and time). This cooperative driving framework can also be extended to a larger transportation network, where the route choice decisions are integrated.

CRediT authorship contribution statement

Zhen Yang: Methodology, Formal analysis, Validation, Investigation, Data curation, Writing - original draft. **Yiheng Feng:** Conceptualization, Methodology, Investigation, Data curation, Funding acquisition, Writing - review & editing. **Henry X. Liu:** Conceptualization, Funding acquisition, Supervision, Writing - review & editing.

Acknowledgement

This research was partially funded by the US Department of Transportation (USDOT) Region 5 University Transportation Center: Center for Connected and Automated Transportation (CCAT) of the University of Michigan. The energy consumption analysis of this paper uses the Michigan MOVES data, which is processed and calibrated by Dr. Guoyuan Wu at the University of California, Riverside.

Appendix A

Variables and Notations

Variables	Meaning	Unit
General Notations		
i	Intersection index.	
j	Lane index.	
ϕ	Signal phase index. A lane-to-phase mapping $\phi = f(j)$ maps a lane to its corresponding phase. In the ring-barrier diagram, $\phi_{\beta\gamma\sigma}$ is used to indicate that the phase belongs to ring β, barrier γ. When $\sigma = 1$, the phase is the lead phase, and when $\sigma = 0$, the phase is the lag phase.	
k	Vehicle group index within a lane. A CAV platoon, a single CV or a single RV is considered as a vehicle group.	
s	Vehicle position index within a vehicle group. For a single CV or RV, $s = 1$.	
Vehicle level model Parameters		
v	Vehicle current speed	m/s
Δd	Distance to the front vehicle. The front vehicle is defined as the immediate downstream vehicle.	m
$\widetilde{v}$	Speed of the front vehicle.	m/s
$\widetilde{a}$	Acceleration of the front vehicle.	m/s^2
a^{+}_{max}	Maximum acceleration	m/s^2
$a^{-}_{comfort}$	Comfortable deceleration	m/s^2
$\overline{v}$	Average speed during the trigonometric trajectory planning period	m/s
v^0	Initial vehicle speed of the trigonometric eco-trajectory planning period	m/s
a^0	Initial acceleration of the trigonometric eco-trajectory planning period	m/s^2
d^{stop}	Distance to the stop bar	m
t^{arr}	Time of arrival at the stop bar.	s
m, n	Model parameters. Detailed explanation can be found in (Barth et al., 2011)	
$jerk_{max}$	Maximum allowed jerk	m/s^3
v^{max}	Speed limit.	
Γ	Green window during which a vehicle can pass the intersection	s
t^{leave}	Time interval from the start of the green to the time when the front vehicle leaves the intersection.	s
t^{queue}	Time when the vehicle arrives at the end of the queue	s
t^{e}	Earliest time the vehicle can arrive at the stop bar	s
Intersection level model parameters		
Decision Variables		
D_{jks}	Delay of the sth vehicle in vehicle group k in lane j	s
N_{jk}	Number of CAVs in vehicle group k in lane j	
θ_{ϕ}	Green split of phase ϕ.	s
g^{rem}_{ϕ}	Remaining green time of phase ϕ.	s
r^{rem}_{ϕ}	Remaining red time of phase ϕ.	s
u^{g}_{jks}	Binary variable that indicates whether the sth vehicle in vehicle group k in lane j can pass the intersection or not when the approaching phase $\phi = f(j)$ is green	
u^{r}_{jks}	Binary variable that indicates whether the sth vehicle in vehicle group k in lane j can pass the intersection or not when the approaching phase $\phi = f(j)$ is red	
Parameters		
h_{CACC}	Headway between two CAVs (i.e., CACC headway)	s
h_{RV}	Headway between two regular vehicles (i.e., car-following headway)	s
d^{detect}_{j}	Distance from the loop-detector to the stop bar in lane$j$	m
Δt^{detect}_{jks}	Elapsed time after the sth vehicle in vehicle group k in lane j passes the loop detector	s
C	A common cycle length	s
g^{elps}_{ϕ}	Green elapsed time of phase ϕ if it is green and 0 if the phase is red	s
r^{elps}_{ϕ}	Red elapsed time of phaseϕ if it is red and 0 if the phase is green	s
t^{lost}_{ϕ}	Lost time of phase ϕ.	s
I^{g}_{ϕ}	Binary parameter. 1 if phase ϕ is green, and 0 otherwise.	
I^{CACC}_{jk}	Binary parameter. 1 if vehicle group k in lane j consists of CAVs and 0 otherwise	
$t^{ge}_{i\phi}$	End of green time of the phase ϕ at intersection$i$	s
N_{veh}	Number of vehicles at the intersection	
N_{phase}	Number of phases at the intersection	
$N_{platoon}$	Number of platoons at the intersection	
Corridor level model parameters		
Decision Variables		
$\xi_{i,i+1}$	Offset of the coordinated phase from intersection i to intersection $i+1$.	s
$\alpha_{i\phi^*}$	Arrival time of the first vehicle in the primary platoon of coordinated phase ϕ^* of intersection i.	s
D_w	Link performance function of scenario w.	s
Parameters		
$\overline{g}_{i\phi^*}$	Average green split of coordinated phase ϕ^* of intersection i. (i.e., $\phi^* = 2$ for phase 2 and $\phi^* = 6$ for phase 6)	s

(*continued on next page*)

(*continued*)

Variables	Meaning	Unit
$\bar{r}_{i\phi^*}$	Average red duration of coordinated phase ϕ^* of intersection i.	s
$t_{i\phi^*}^{start}$	Start time of coordinated phase ϕ^* of intersection i.	s
$\delta_{i\phi^*}$	Upper bound of offset adjustment of coordinated phase ϕ^* of intersection i.	s
$t_{i,i+1}^{travel}$	Free flow travel time from intersection i to intersection $i+1$.	s
$q_{i\phi^*}$	Current queue length of coordinated phase ϕ^* of intersection i.	m
$q_{i\phi^*}^{'}$	Queue length at the start of the green of coordinated phase ϕ^* of intersection i.	m
$V_{i\phi^*}$	Average volume of coordinated phase ϕ^* of intersection i.	vph
$\Psi_{i\phi^*}$	Number of vehicles in the primary platoon of coordinated phase ϕ^* of intersection i.	
$e_{i\phi^*}$	Time point when the secondary platoon of coordinated phase ϕ^* of intersection i is fully discharged.	s
$p_{i\phi^*}$	Platoon length in time (s) of coordinated phase ϕ^* of intersection i.	s
$y_{i\phi^*}$	V/C ratio of coordinated phase ϕ^* of intersection i.	%
$\zeta_{i\phi^*}$	Right turning ratio of the approach containing the coordinated phase ϕ^* of intersection i.	%
$\xi_{i\phi^*}$	Left turning ratio of the approach containing the coordinated phase ϕ^* of intersection$i$	%
N_{inter}	Number of intersections in the system	

References

Al Islam, S.B., Hajbabaie, A., 2017. Distributed coordinated signal timing optimization in connected transportation networks. Transport. Res. Part C: Emerg. Technol. 80, 272–285.

Almannaa, M.H., Chen, H., Rakha, H.A., Loulizi, A., El-Shawarby, I., 2019. Field implementation and testing of an automated eco-cooperative adaptive cruise control system in the vicinity of signalized intersections. Transport. Res. Part D: Transp. Environ. 67, 244–262.

America, P.T.V., 2014. PTV VISTRO User Manual. Ptv Ag 2, 07.

Barth, M., Mandava, S., Boriboonsomsin, K., Xia, H., 2011. Dynamic ECO-driving for arterial corridors. In: 2011 IEEE Forum on Integrated and Sustainable Transportation Systems. IEEE, pp. 182–188.

Beak, B., Head, K.L., Feng, Y., 2017. Adaptive coordination based on connected vehicle technology. Transp. Res. Rec. 2619 (1), 1–12.

Feng, Y., Head, K.L., Khoshmagham, S., Zamanipour, M., 2015. A real-time adaptive signal control in a connected vehicle environment. Transport. Res. Part C: Emerg. Technol. 55, 460–473.

Feng, Y., Yu, C., Liu, H.X., 2018. Spatiotemporal intersection control in a connected and automated vehicle environment. Transport. Res. Part C: Emerg. Technol. 89, 364–383.

Feng, S., Zhang, Y., Li, S.E., Cao, Z., Liu, H.X., Li, L., 2019. String stability for vehicular platoon control: Definitions and analysis methods. Ann. Rev. Control.

Feng, S., Sun, H., Zhang, Y., Zheng, J., Liu, H.X., Li, L., 2019. Tube-based discrete controller design for vehicle platoons subject to disturbances and saturation constraints. IEEE Trans. Control Syst. Technol.

Feng, Y., 2015. Intelligent traffic control in a connected vehicle environment.

Gartner, N.H., Little, J.D., Gabbay, H., 1975. Optimization of traffic signal settings by mixed-integer linear programming: Part I: The network coordination problem. Transport. Sci. 9 (4), 321–343.

Goodall, N.J., Smith, B.L., Park, B., 2013. Traffic signal control with connected vehicles. Transp. Res. Rec. 2381 (1), 65–72.

Guo, Y., Ma, J., Xiong, C., Li, X., Zhou, F., Hao, W., 2019. Joint optimization of vehicle trajectories and intersection controllers with connected automated vehicles: Combined dynamic programming and shooting heuristic approach. Transport. Res. Part C: Emerg. Technol. 98, 54–72.

He, X., Liu, H.X., Liu, X., 2015. Optimal vehicle speed trajectory on a signalized arterial with consideration of queue. Transport. Res. Part C: Emerg. Technol. 61, 106–120.

Kamal, M.A.S., Hayakawa, T., Imura, J.I., 2019. Development and Evaluation of an Adaptive Traffic Signal Control Scheme Under a Mixed-Automated Traffic Scenario. IEEE Trans. Intell. Transp. Syst.

Kesting, A., Treiber, M., Helbing, D., 2010. Enhanced intelligent driver model to access the impact of driving strategies on traffic capacity. Philos. Trans. Royal Soc. A: Mathem., Phys. Eng. Sci. 368 (1928), 4585–4605.

Koupal, J., Cumberworth, M., Michaels, H., Beardsley, M., Brzezinski, D., 2003. Design and implementation of MOVES: EPA's new generation mobile source emission model. Ann. Arbor. 1001 (48), 105.

Li, Z., Elefteriadou, L., Ranka, S., 2014. Signal control optimization for automated vehicles at isolated signalized intersections. Transport. Res. Part C: Emerg. Technol. 49, 1–18.

Li, S.E., Zheng, Y., Li, K., Wang, J., 2015. An overview of vehicular platoon control under the four-component framework. In: 2015 IEEE Intelligent Vehicles Symposium (IV). IEEE, pp. 286–291.

Liang, X.J., Guler, S.I., Gayah, V.V., 2020. A heuristic method to optimize generic signal phasing and timing plans at signalized intersections using Connected Vehicle technology. Transport. Res. Part C: Emerg. Technol. 111, 156–170.

Liu, H., Lu, X.Y., Shladover, S.E., 2019. Traffic signal control by leveraging Cooperative Adaptive Cruise Control (CACC) vehicle platooning capabilities. Transport. Res. Part C: Emerg. Technol. 104, 390–407.

Optimization, G., 2014. Inc., Gurobi optimizer reference manual, 2015.

PTV, A., 2014. PTV VISSIM 7 user manual. PTV Group, Haid-und-Neu-Str, 15.

Sharma, A., Bullock, D.M., Bonneson, J.A., 2007. Input–output and hybrid techniques for real-time prediction of delay and maximum queue length at signalized intersections. Transp. Res. Rec. 2035 (1), 69–80.

Van Arem, B., Van Driel, C.J., Visser, R., 2006. The impact of cooperative adaptive cruise control on traffic-flow characteristics. IEEE Trans. Intell. Transp. Syst. 7 (4), 429–436.

Wang, Z., Wu, G., Hao, P., Boriboonsomsin, K., Barth, M., 2017. Developing a platoon-wide eco-cooperative adaptive cruise control (CACC) system. In: 2017 IEEE Intelligent Vehicles Symposium (IV). IEEE, pp. 1256–1261.

Wu, X., Liu, H.X., 2011. A shockwave profile model for traffic flow on congested urban arterials. Transport. Res. Part B: Methodol. 45 (10), 1768–1786.

Xu, B., Ban, X.J., Bian, Y., Li, W., Wang, J., Li, S.E., Li, K., 2018. Cooperative method of traffic signal optimization and speed control of connected vehicles at isolated intersections. IEEE Trans. Intell. Transp. Syst. 20 (4), 1390–1403.

Yang, Z., Feng, Y., Gong, X., Zhao, D. and Sun, J., 2019. Eco-Trajectory Planning with Consideration of Queue along Congested Corridor for Hybrid Electric Vehicles. Transport. Res. Record, p. 0361198119845363.

Yang, H., Rakha, H., Ala, M.V., 2016. Eco-cooperative adaptive cruise control at signalized intersections considering queue effects. IEEE Trans. Intell. Transp. Syst. 18 (6), 1575–1585.
Yu, C., Feng, Y., Liu, H.X., Ma, W., Yang, X., 2018. Integrated optimization of traffic signals and vehicle trajectories at isolated urban intersections. Transport. Res. Part B: Methodol. 112, 89–112.
Yu, C., Feng, Y., Liu, H.X., Ma, W., Yang, X., 2019. Corridor level cooperative trajectory optimization with connected and automated vehicles. Transport. Res. Part C: Emerg. Technol. 105, 405–421.